



XVII International Colloquium on Mechanical Fatigue of Metals (ICMFM17)

## Strain accumulation in TiAl intermetallics via high-resolution Digital Image Correlation (DIC)

C. Içöz<sup>a</sup>, L. Patriarca<sup>a,b</sup>, M. Filippini<sup>a,\*</sup>, S. Beretta<sup>a</sup>

<sup>a</sup>Politecnico di Milano, Dipartimento di Meccanica, Via La Masa 1, 20156 Milano

<sup>b</sup>University of Illinois at Urbana-Champaign, Dept. of Mechanical Science and Engineering, 1206 W. Green St., Urbana, IL 61801, USA

### Abstract

Novel manufacturing processes are more and more used to produce advanced structural materials such as the gamma titanium aluminide alloys ( $\gamma$ -TiAl). In this work we examine a Ti-48Al-2Cr-2Nb alloy obtained with an additive manufacturing technique by Electron Beam Melting (EBM) by conducting monotonic and cyclic loading experiments both on tension and compression samples to investigate the influence of the microstructure in strain accumulation process by fatigue loading. The residual strain maps corresponding to different applied stress levels, number of cycles and microstructures are obtained through the use of high-resolution Digital Image Correlation (DIC). The strain maps were overlaid with the images of the microstructure and detailed analyses were performed to investigate the features of the microstructure where high local strain heterogeneities arise. Such experiments, conducted ex-situ at room temperature, allow to characterize the effect of different microstructures on the strain accumulation process, providing additional information into the effect of the lamellar and equiaxed grains and also to capture the evolution of the local deformation process for TiAl. The measure of the residual strains provides further information on the role of the intermetallic phases on the fatigue behavior of  $\gamma$ -TiAl alloys. The comparison with the strain accumulation in fully lamellar microstructure with larger grain size permits to highlight the influence of the position of grain boundaries and the orientation of the lamellae for the onset of fatigue cracking. The analysis and comparison of the strain maps provide information for the selection of the microstructural parameters during material design (i.e. grain size and lamellar grains volume fraction).

© 2014 Elsevier Ltd. Open access under [CC BY-NC-ND license](https://creativecommons.org/licenses/by-nc-nd/4.0/).

Selection and peer-review under responsibility of the Politecnico di Milano, Dipartimento di Meccanica

**Keywords:** Mechanisms of early fatigue damage; Digital Image Correlation; TiAl intermetallics

### Introduction

In order to design mechanical components made of intermetallic  $\gamma$ -TiAl alloys produced with advanced manufacturing processes, a deep understanding of the damage accumulation process in the microstructure is required, for identifying suitable process routes to obtain the required structural integrity of the components. In the last decades more and more efforts have been devoted in understanding the effect of the local microstructure on the deformation of  $\gamma$ -TiAl alloys. Even though the investigations at the micro-scales provide useful information on the microscopic defor-

\* Corresponding author. Tel.: +39-02-2399-8220 ; fax: +39-02-2399-8202.

E-mail address: [mauro.filippini@polimi.it](mailto:mauro.filippini@polimi.it)

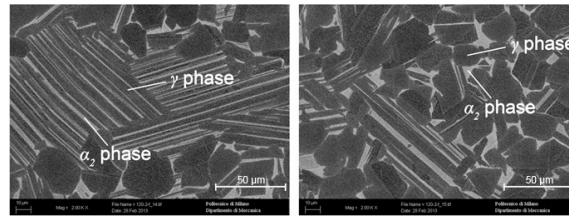


Fig. 1. Micrographs captured through scanning electron microscopy showing the typical microstructure of the  $\gamma$ -TiAl alloy used in this work.

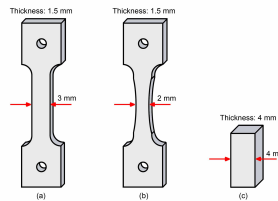


Fig. 2. Specimen geometries adopted in this study: (a) tensile monotonic experiment; (b) tensile fatigue experiment. (c) compressive monotonic and fatigue experiments.

mation mechanisms [1,2], there is the need to develop experimental tools for investigating the deformation behavior of these alloys at larger scales, which include several grains, still capturing the effect of the local microstructure. Using advanced optical techniques, in this work we investigate the origin of the strain heterogeneities in duplex  $\gamma$ -TiAl alloys by analyzing the strain fields originated from different microstructures (lamellar and equiaxed grains) for compressive and tensile loadings.

The adoption of additive manufacturing processes such as Electron Beam Melting (EBM) for material production avoids the typical defects that are introduced in the material by conventional processes, e.g. by investment casting. Thus, there's the need to understand how microstructure influences where high local strain heterogeneities arise and subsequently promote crack nucleation. The fatigue strength of  $\gamma$ -TiAl alloy is strongly influenced by the size, orientation and distribution of lamellar colonies [1,3]. In the present work, the deformation of  $\gamma$ -TiAl alloy is investigated using local strain field measurements via DIC technique [4], in conjunction with the information of the local microstructure. Such experimental tool allows to characterize the effect of different microstructures on the damage accumulation process providing additional information into the effect of the lamellar and equiaxed grains.

## 1. Material and sample geometry

The  $\gamma$ -TiAl alloy adopted in this work has a composition of 48% of Al, 2% of Cr and 2% of Nb content (atomic percentages). The material was produced by additive manufacturing through EBM A2 machine produced and distributed by Arcam AB (Sweden), [5]. After the material manufacturing, the ingots were hot isostatically pressed (HIPed) at 1260 °C under a pressure of 1700 bar for 4 h. The final duplex microstructure was obtained by means of a heat treatment at 1320 °C for 2 h [6]. The typical duplex microstructure obtained using Back-Scattered images in the Scanning Electron Microscope (SEM) is shown in Fig. 1. Lamellar grains are composed by several layers of  $\gamma$ -phase and  $\alpha_2$ -phase in the form of platelets. The core of the equiaxed grains is mainly composed by the  $\gamma$ -phase, while the  $\alpha_2$ -phase typically settles at the equiaxed grain boundaries. Depending on the cooling rate some of the samples display a predominant lamellar structure, which enable the comparison between the local deformation of different microstructures as shown later in this paper.

The samples were cut by wire Electro-Discharge Machining (EDM) in three different specimen geometries, Fig. 2. The original samples were then sectioned into dog-bone shaped specimens for the experiments in tension: with parallel gauge section for monotonic loading (1.5 mm  $\times$  3 mm cross-section, Fig. 2a), and with hourglass shape for fatigue loading (1.5 mm  $\times$  2 mm cross-section, see Fig. 2b). The compression specimens were sectioned into 4 mm  $\times$  4 mm  $\times$  10 mm, and the same geometry was used for both monotonic (static) and fatigue experiments, Fig. 2c.

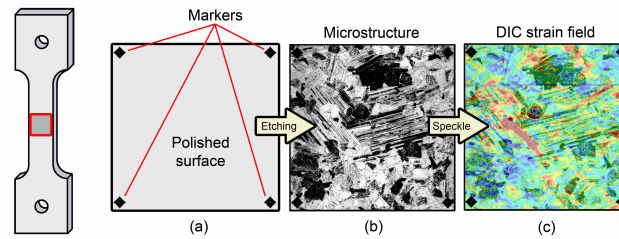


Fig. 3. Specimen preparation, positioning of fiducial markers (a), microstructure observation after etching (b) and final strain map example (c) for a sample loaded in tension.

## 2. Local strain measurements

Local strain fields were obtained through DIC technique and combined with local microstructure [7]. The samples were initially polished using SiC paper (from P800 up to P2500), and the final surface finish was then obtained using diamond pastes. Indentation by Vickers marks was used in order to define a target region on the sample's surface (see Fig. 3a). The typical area analyzed in this work corresponds to a  $1 \text{ mm} \times 1 \text{ mm}$  square region. In order to characterize the local microstructure, the samples were etched [8] to reveal the microstructure in the region under observation, Fig. 3b. The markers are located on the sample's surface after the etching. Then, a speckle pattern adapted for high resolution ex-situ DIC was produced on the sample's surface. The fine speckle allows to capture images at a resolution of  $0.17 \mu\text{m}/\text{pixel}$  by means of a Carl Zeiss Axio Cam A1 optical microscope with a Carl Zeiss ERc5s camera. The images were captured out of the load frame (unloaded condition) before the experiment (reference images), and after one or more load cycles (deformed images). The reference and deformed images were successively correlated, in order to obtain the strain field of the marked region. The correlation was performed by using the VIC-2D software, allowing high strain resolution depending on the quality of the images. The overlap between the microstructure and the strain fields allows to create the strain maps correlated with the microstructure as depicted in Fig. 3c. The samples were cyclically loaded in tension (Fig. 2b) at room temperature using an MTS Acumen electrodynamic test machine. For all the other sample geometries (monotonic and cyclic experiments in compression, Fig. 2c, and monotonic experiments in tension, Fig. 2a) a servo-hydraulic MTS 810 testing machine was used. The samples for fatigue experiments were loaded at a fixed stress ratio of  $R = |\sigma_{\min}|/|\sigma_{\max}| = 0.05$  in stress control at frequencies contained in the range (1-10) Hz depending on the loading direction.

## 3. Experiments and strain localization analysis

### 3.1. Monotonic experiments

Stress-strain curves obtained from two monotonic (static) experiments in tension and two in compression are shown in Fig. 4. The experiments in tension were carried out in strain control, while the experiments in compression in displacement control. The images were captured during the loading, and the strain maps of the axial strain ( $\epsilon_{yy}$ ) were successively averaged. In Fig. 4, the monotonic stress-strain curves are derived by combining the DIC average (longitudinal) measured strain and the stress measured during the tests, both in tension and in compression. The deformation in tension is limited, and the maximum stress never exceeds  $\sigma_{\text{nom}} = 400 \text{ MPa}$ . In compression tests, more ductility was observed and higher stresses and strains were attained. The observed asymmetric yield behavior of TiAl is consistent with other works reported in the literature, see [9] and [10, p. 99].

### 3.2. Fatigue experiments in compression

The analysis of the deformation of a sample cyclically loaded in compression at a defined nominal maximum stress of  $\sigma_{\text{nom}} = 390 \text{ MPa}$  required to attain plasticity in the sample is shown in Fig. 5. The deformed images were

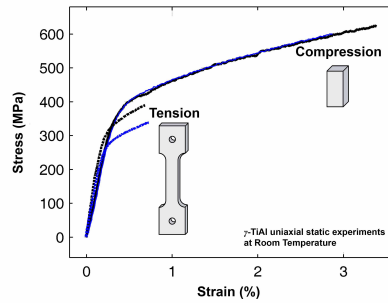


Fig. 4. Stress-strain curves obtained from monotonic (static) experiments both in tension and compression.

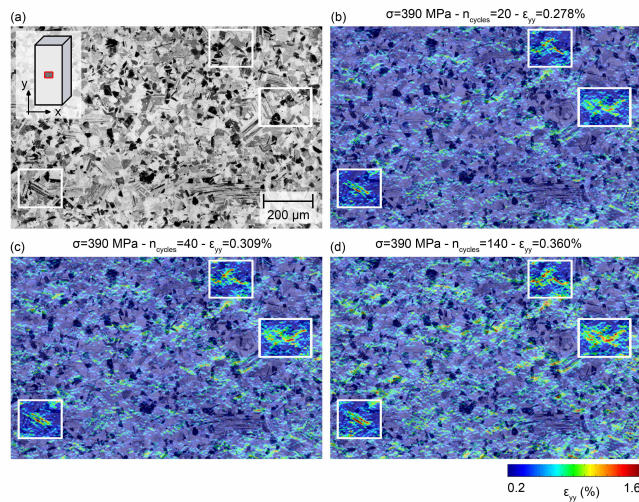


Fig. 5. Local strain accumulation obtained ex-situ for a sample cyclically loaded in compression at a nominal stress of  $\sigma_{nom} = 390$  MPa.

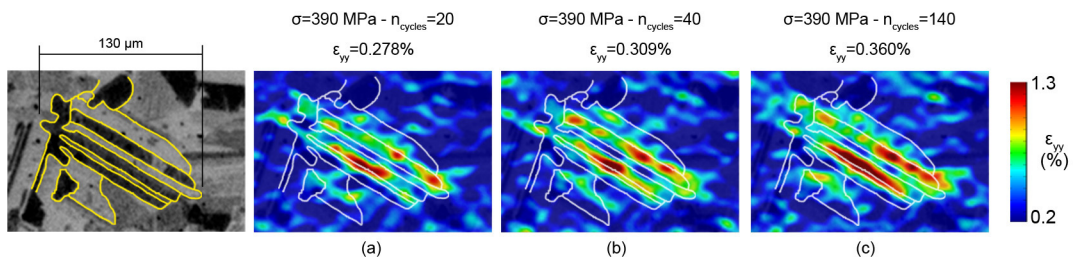


Fig. 6. High resolution DIC (ex-situ) for a lamellar grain captured from the strain map reported in Figure 5. Strains accumulate inside the defined lamellar platelets which are composed by the  $\gamma$ -TiAl phase.

captured after 20, 40 and 140 cycles. Here, the maximum compressive stress applied is approximately equal in magnitude to the ultimate tensile stress. All the strain fields given in Fig. 5 display to the axial strain in the load direction ( $\epsilon_{yy}$ ) overlapped with the local microstructure. The local strain fields show high local strain heterogeneities, which are approximately 3-4 times higher than the average axial strain. Moreover, Fig. 5 illustrates that the strains preferentially accumulates in proximity of specific microstructural features. Fig. 6 shows the lamellar grain that displays the largest strain localizations measured from the experiment depicted in Fig. 5. It can be observed that the largest strain heterogeneities were measured along two defined lamellae platelets, which are composed by the

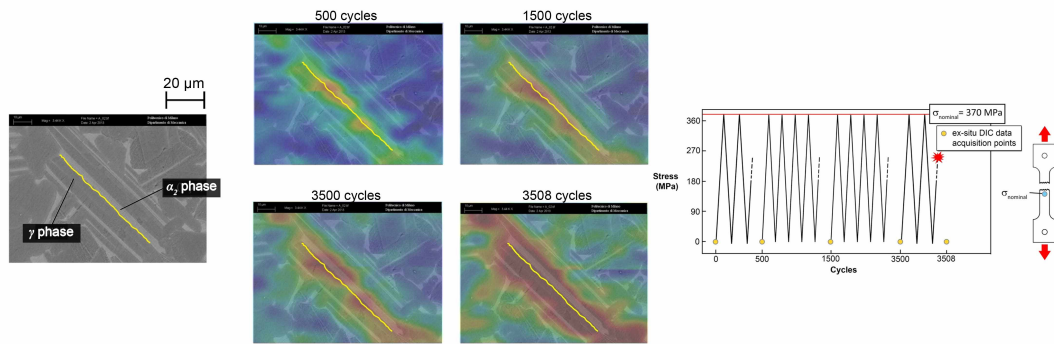


Fig. 7. High resolution strain field (ex-situ) for a lamellar region combined with the microstructure characterization from BSE.

$\gamma$ -phase. The high strain gradients that form in some of the lamellae platelets could potentially generate sites for crack nucleation due to high stresses induced by the accumulation of dislocations at the grain boundary.

### 3.3. Fatigue experiments in tension

The analysis of the deformation of a lamellar grain in a tensile sample cyclically loaded at a nominal maximum stress of  $\sigma_{nom} = 370$  MPa is shown in Fig. 7. The sample failure occurred after 3508 cycles. The fatigue experiment was stopped three times (after 500, 1500 and 3500 cycles) in order to remove the sample from the load frame and capture the images using the DIC technique. In Fig. 7, back scatter electron (BSE) was used to capture the image of a lamellar grain. The dark grey corresponds to the  $\gamma$  phase, while the light grey corresponds to the  $\alpha_2$  phase. Since all the lamellar grains are mainly composed by the  $\gamma$  phase, and the lamellae have a favorable orientation (the normal of the lamellar grain projected on the DIC surface is approximately  $45^\circ$  respect to the loading direction), almost all the lamellar grains yield and display large values of local residual axial strains.

### 3.4. Additional experiments in tension with fully lamellar (FL) microstructure

Additional experiments in tension were carried out on samples characterized by different microstructures. In particular, samples with fully lamellar (FL) microstructure with large lamellar colony sizes were obtained by changing the heat treatment parameters of the same  $\gamma$ -TiAl alloy object of the present paper. Tensile test up to 370 MPa and subsequent DIC analysis, Fig. 8, reveal that for a FL microstructure, strain heterogeneities appear immediately in lamellar grains unfavorably oriented respect to the loading direction. Moreover, strain localization becomes evident also at colony boundaries, due to impossibility to accommodate strains across differently oriented lamellar colonies, as it can be observed in the DIC analysis shown in Fig. 8.

## 4. Discussion and conclusions

In this work high resolution strain measurements through the DIC technique were adopted in order to characterize the deformation behavior of a  $\gamma$ -TiAl alloy under static and fatigue loadings. Detailed microstructural images and strain maps at grain level are provided for different microstructures. Independently from the loading direction (tension versus compression) high strain localizations were measured within the lamellar grains (see Fig. 5–7). These results confirm and support the conclusions of a previous study on the same alloy [3], and from the general literature on duplex TiAl alloys [10,11] in which the lamellar grains are considered the intrinsic initial defects that govern the first stages of crack initiation.

Overlapping of the strain maps with BSE images allowed the identification of the TiAl phases that are mostly involved in the strain accumulation mechanism. Fig. 6 shows the strain localization inside two defined lamellar platelets contained in the lamellar colony for a sample loaded in compression. The deformation is localized initially

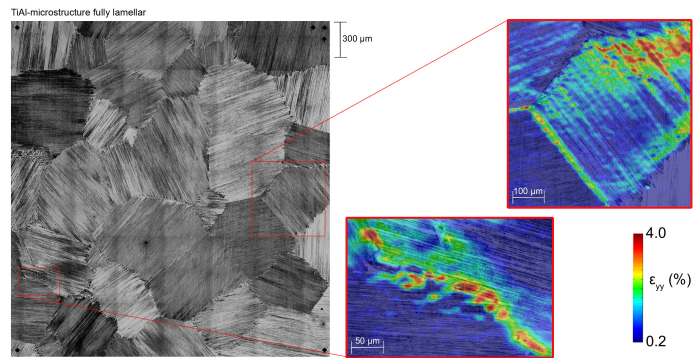


Fig. 8. High resolution DIC strain measurements obtained ex-situ in tension at a nominal stress of  $\sigma_{nom} = 370$  MPa for a fully lamellar microstructure with large lamellar colonies.

in two lamellae, and cyclically accumulates inside the same grains. The same behavior is observed in tension (Fig. 7). It can be stated that the accumulation of local strains at a grain boundary could promote crack initiation because of the strain heterogeneity across the interface [1,12]. This observation is consistent with the observations of the microstructural deformation mechanisms leading to crack nucleation (slip incompatibilities and twin blockage at the grain boundaries), [12]. A preliminary result for a fully lamellar microstructure with large colonies shows that increasing the lamellar grain size is detrimental in FL microstructures, because higher strain localizations are observed both in the unfavorable oriented colonies and at the grain boundaries. Further studies are needed to analyze the effect of the lamellar grain size which is believed to play a significant role in the fatigue resistance of  $\gamma$ -TiAl alloys.

## References

- [1] K. S. Chan, D. S. Shih, Fundamental aspects of fatigue and fracture in a TiAl sheet alloy, *Metal. Mater. Trans. A* 29 (1998) 73–87.
- [2] A.-L. Gloanec, G. Henaff, M. Jouiad, D. Bertheau, P. Belaygue, M. Grange, Cyclic deformation mechanisms in a gamma titanium aluminide alloy at room temperature, *Scripta Mat.* 52 (2005) 107–111.
- [3] M. Filippini, S. Beretta, L. Patriarca, G. Pasquero, S. Sabbadini, Defect tolerance of a gamma titanium aluminide alloy, *Proc. Eng.* 10 (2011) 3677–3682.
- [4] M. A. Sutton, J.-J. Orteu, H. W. Schreier, *Image Correlation for Shape, Motion and Deformation Measurements*, Springer-Verlag, Heidelberg, 2009.
- [5] L.-E. Andersson, M. Larsson, Device and arrangement for producing a three-dimensional object, Patent Application, 2001. WO 2001/081031 A1.
- [6] S. Biamino, A. Penna, U. Ackelid, S. Sabbadini, O. Tassa, P. Fino, M. Pavese, P. Gennaro, C. Badini, Electron beam melting of Ti-48Al-2Cr-2Nb alloy: Microstructure and mechanical properties investigation, *Intermetallics* 19 (2011) 776–781.
- [7] J. Carroll, W. Abuzaid, J. Lambros, H. Sehitoglu, An experimental methodology to relate local strain to microstructural texture, *Rev. Sci. Instr.* 81 (2010) 083703.
- [8] W. A. Baeslack III, P. A. McQuay, D. S. Lee, E. D. Fletcher, Metallography of gamma titanium aluminides, *Mat. Char.* 31 (1993) 197–207.
- [9] M. Zupan, K. J. Hemker, Yielding behavior of aluminum-rich single crystalline  $\gamma$ -TiAl, *Acta Mater.* 51 (2003) 6277–6290.
- [10] F. Appel, J. D. H. Paul, M. Oehring, *Gamma Titanium Aluminide Alloys: Science and Technology*, Wiley-VCH Verlag GmbH & Co., Weinheim, Germany, 2011.
- [11] F. Appel, M. Oehring, Titanium aluminide alloys: Alloy design and properties, in: C. Leyens, M. Peters (Eds.), *Titanium and Titanium Alloys*, Wiley-VCH Verlag GmbH & Co., Weinheim, Germany, 2005, pp. 89–152.
- [12] T. R. Bieler, P. Eisenlohr, F. Roters, D. Kumar, D. E. Mason, M. A. Crimp, D. Raabe, The role of heterogeneous deformation on damage nucleation at grain boundaries in single phase metals, *Int. J. Plast.* 25 (2009) 1655–1683.